

Electron dynamics and injection in plasma-based accelerators with sharp vacuum-plasma transitions

Ronghao Hu,¹ Haiyang Lu,^{1,2,*} Yinren Shou,¹ Jinqing Yu,¹ Chia-erh Chen,¹ and Xueqing Yan^{1,2,†}

¹*State Key Laboratory of Nuclear Physics and Technology,
and Key Laboratory of HEDP of the Ministry of Education,
CAPT, Peking University, Beijing 100871, China*

²*Collaborative Innovation Center of Extreme Optics,
Shanxi University, Taiyuan, Shanxi 030006, China*

(Dated: December 12, 2021)

The dynamic process of a laser or particle beam propagating from vacuum into underdense plasma has been investigated theoretically. Our theoretical model combines a Lagrangian fluid model with the classic quasistatic wakefield theory. It is found that background electrons can be injected into wakefields because sharp vacuum-plasma transitions can reduce the injection threshold. The injection condition, injection threshold as well as the injection length can be given theoretically by our model and are compared with results from computer simulations. Moreover, electron beams of high qualities can be produced near the injection thresholds and the proposed scheme is promising in reducing the injection threshold and improving the beam qualities of plasma based accelerators.

Plasma acceleration is a fast-developing technique for accelerating charged particles with plasma waves driven by laser or particle beams. Current experiments have shown accelerating gradients several orders of magnitude higher than conventional particle accelerators[1], offering a way to build high performance particle accelerators of much smaller size. The basic concepts of laser wakefield accelerator (LWFA) were first proposed by T. Tajima and J. M. Dawson in 1979[2], where electrons are accelerated by plasma waves driven by laser pulses. Several years later, P. Chen *et al*[3] proposed the concepts of plasma wakefield accelerator (PWFA) where high current electron bunches are used to generate intense electric fields to accelerate trailing copropagating electron bunches. Experimental breakthroughs[1, 4–10] has been made in recent years and electron energy gain was improved to 4.2 GeV in LWFA[10] and over 40 GeV in PWFA[6]. Several injection scheme were proposed and investigated, including self-injection[11–15], downramp injection[16–18], colliding pulse injection[19–23] and ionization injection[24–33]

Despite the great achievements made in the past few decades, we are still far from fully understanding the physics of plasma acceleration. For example, the dynamic process of a laser or particle beam propagating from vacuum into underdense plasma still lacks investigation. The classic quasistatic wakefield theory treats the drivers as if they were born inside the plasmas and the boundary effects are neglected[1]. Natural gas plasmas produced by gas jets have boundary density ramps with lengths from hundreds of microns to millimeters[34]. Quasistatic theory is applicable in this case because the density changes slowly as the driver propagates. Several techniques[18, 34, 35] have been proposed to produce sharp density transitions with transition ramp

lengths about tens of microns, which are comparable to the plasma wavelengths used for acceleration[1] and the wavelengths of mid-infrared lasers (10.6 μm for CO₂ laser). For these sharp density transitions, quasistatic theory needs to be modified to comprehend the underlying physics.

In this letter, we introduce a theoretical model to investigate the dynamic process of a laser or particle beam propagating from vacuum into plasma. A Lagrangian fluid model[36] combined with quasistatic wakefield theory can give us a clear physical picture of this dynamic process. We found that the main differences between sharp transitions and long transitions are the behaviors of a group of electrons that can enter the vacuum and return to the plasma. Some of these refluxing electrons can be injected into the wakefields and get accelerated. The dynamics of refluxing electrons and a theoretical derivation of the injection condition, injection threshold and injection length of refluxing electron injection (REI) are discussed in the following. Theoretical results are compared with numerical results from 1D and 3D particle-in-cell (PIC) simulations with EPOCH[37], showing that our model have included the essence of the underlying physics. The injection threshold of REI is also found to be smaller than that of self-injection[14]. The beam qualities of REI are characterized with 3D PIC simulations and it is found that high quality electron beams can be generated near the injection thresholds.

For laser drivers and cold plasmas, the 1D equations of motion averaged by laser cycles can be given as[1]

$$\frac{dp_x}{dt} = -E + F_p, \quad \frac{dx}{dt} = p_x/\gamma. \quad (1)$$

t is time normalized by ω_p^{-1} , where $\omega_p = \sqrt{n_e e^2 / m_e \epsilon_0}$ is the plasma frequency, n_e is plasma density, e is elementary charge, m_e is electron mass at rest and ϵ_0 is vacuum permittivity. p_x is the longitudinal momentum and is normalized by $m_e c$, where c is the light

* hylu@pku.edu.cn

† x.yan@pku.edu.cn

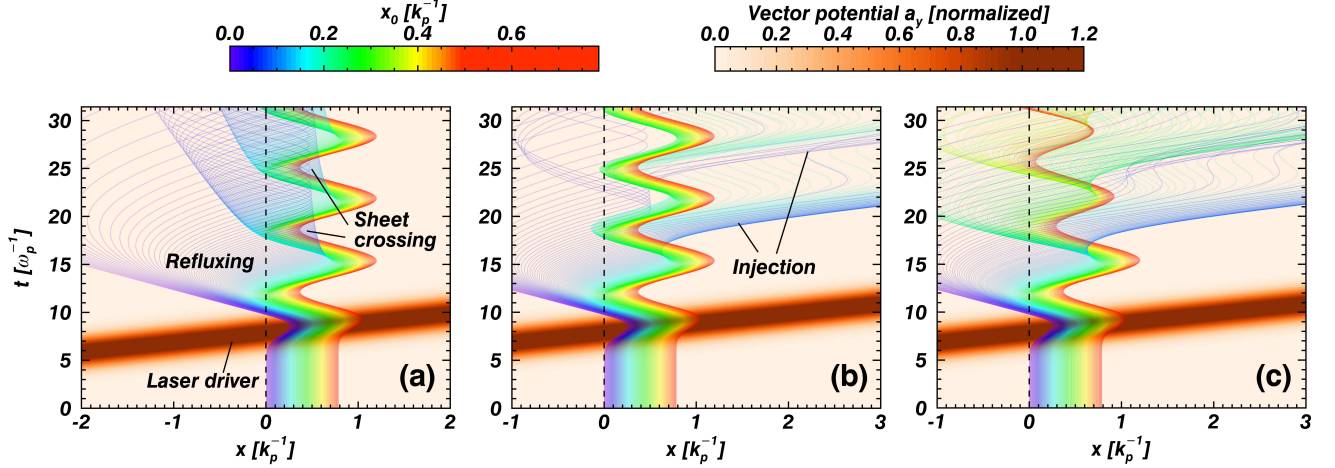


FIG. 1. Trajectories of electrons with different initial positions marked with different colors. (a) Numerical solutions of equations (1) without modifications after sheet crossing. (b) Numerical solutions including quasistatic theory after sheet crossing. (c) Trajectories obtained from a PIC simulation with the same parameters. The filled contour plots in each subfigure show the spatiotemporal profiles of the driving laser and the dashed lines indicate the initial plasma boundary. The laser is incident from left to right, and plasma initially locates in the $x > 0$ area. $a_0=1.2$ and $n_0/n_c=0.004$ are used in all subfigures.

velocity in vacuum. x is longitudinal position normalized by k_p^{-1} , where $k_p = \omega_p/c$ is the plasma wavenumber. E is the longitudinal electric field and is normalized by $m_e \omega_p c / e$. $F_p = -\frac{1}{4\gamma} \frac{\partial a^2}{\partial x}$ is the ponderomotive force of a linearly polarized laser driver, normalized by $m_e \omega_p c$, a is the laser vector potential normalized by $m_e c / e$ and $\gamma = \sqrt{1 + a^2/2 + p_x^2}$ is the Lorentz factor. All the physical quantities are in SI units. For particle drivers, one only needs to replace the ponderomotive force with the space charge force and neglect the $a^2/2$ term in the Lorentz factor. Before sheet crossing happens, the order of electron sheets is not disturbed and the electric force can be obtained from Poisson's equation as $E = \int_{-\infty}^x [n_i(x) - n_e(x)] dx = \int_{x_0}^x n_0(x) dx$, where $n_i(x)$ is the positive charge density, $n_e(x)$ is electron density and $n_0(x)$ is the initial undisturbed electron density[36]. Here ions are assumed to be fixed and all the density values are normalized using $n_0(x=0)$. For simplicity without losing generality, the density profile of a vacuum-plasma transition (locates at $x=0$) can be written as $n_0(x) = H(x)$, where $H(x)$ is the unit step function, and the electric force for electrons initially at x_0 can be written as $E = xH(x) - x_0$. Equations (1) can be integrated numerically for a linearly polarized gaussian laser pulse with $a = a_y = a_0 \exp[-(t - x/v_d - t_{delay})^2/\tau^2]$, where a_0 is the peak vector potential, v_d is the velocity of the driver, t_{delay} is the time delay of the pulse peak and τ is the 1/e half pulse duration. For drivers with small amplitudes ($a_0 \sim 1$), $v_d \approx \sqrt{1 - n_0/n_c}$, where n_c is the critical plasma density[1]. Fig. 1(a) shows the numerical solutions of equations (1), where the rainbow-colored wavy lines are particle trajectories moving in the laser and charge separation fields, with colors being the initial

positions of the particles, x_0 , given by the color bar on top. Some particles (like red ones in Fig. 1(a)) oscillate and remain approximately the same region in the plasma while the laser moves forward into the plasma. Electrons near the boundary (the blue ones in the back) are ejected into the vacuum, and sheet crossing[36], or the crossing of electron trajectories happens shortly after they re-enter the plasma. Electrons initially deep inside the plasma are oscillating with constant amplitudes and by neglecting the ponderomotive force term in equations (1), one can obtain a constant of motion for the oscillation, i.e. $\mathcal{H} = \sqrt{1 + p_x^2} - \Psi$, where Ψ is the electrostatic potential and $\partial\Psi/\partial x = -E$. An approximate solution for small amplitude oscillation can be obtained as

$$\begin{aligned} p_x(t, x_0) &= -p_m \cos[\omega_\gamma(t - x_0/v_d - t_0)], \\ x(t, x_0) &= x_0 - \delta_m \sin[\omega_\gamma(t - x_0/v_d - t_0)]. \end{aligned} \quad (2)$$

p_m is the maximum oscillation momentum, $\gamma_m = \sqrt{1 + p_m^2}$ is the maximum Lorentz factor after the driver and $\delta_m = \sqrt{2(\gamma_m - 1)}$ is the maximum displacement of the oscillation. t_0 is the time electron with $x_0 = 0$ enters the vacuum. For gaussian drivers with $a_0 \sim 1$, $\tau \approx \pi/2$ and $v_d \sim 1$, we found $\gamma_m \approx 1.005 + 0.166(a_0 - 0.5)^2$. ω_γ is the relativistic oscillation frequency, and can be fitted as $\omega_\gamma \approx \gamma_m^{-0.44}$. For electrons have initial positions $0 < x_0 < \delta_m$, they follow the same oscillation motion until they reach the plasma boundary and then enter the vacuum ($x < 0$), where they experience constant positive electric forces as $E(x) = -x_0$. By this force, they will return to the plasma with a maximum momentum equal to p_m , as shown in Fig. 1(a). The refluxing time, which is defined as the time from the refluxing electron leaving its initial position with negative velocity to its returning, can

be written as $t_{re} = 2 \arccos(p_0/p_m)/\omega_\gamma + 2p_0/x_0$, where $p_0 = \sqrt{(\gamma_m - x_0^2/2)^2 - 1}$ is the electron momentum at $x = 0$. As one can see, the refluxing time t_{re} is a function of the initial position x_0 and its value ranging from π/ω_γ to $+\infty$. For refluxing electrons with proper refluxing time, their trajectories will intersect with the trajectories of oscillating electrons (Fig. 1(a)). The trajectories of refluxing electrons inside the plasma and the trajectory of the outermost oscillating electrons ($x_0 = \delta_m$) will cross on condition that

$$\begin{aligned} x_0 + \delta_m \sin[\omega_\gamma(t_{sc} - x_0/v_d - t_{re} - t_0)] \\ = \delta_m - \delta_m \sin[\omega_\gamma(t_{sc} - \delta_m/v_d - t_0)]. \end{aligned} \quad (3)$$

Solving equation (3), one can obtain the sheet crossing time $t_{sc} = t_0 + x_0/v_d + t_{re} + \arcsin[A/\sqrt{2 + 2\sin(B)} - C]/\omega_\gamma$, where $A = 1 - x_0/\delta_m$, $B = \omega_\gamma[(\delta_m - x_0)/v_d - t_{re}]$, $C = \arcsin[\cos(B)/\sqrt{2 + 2\sin(B)}]$.

Sheet crossing will always happen near the vacuum-plasma transition, but only when the plasma waves are strong enough can refluxing electrons be trapped. After sheet crossing, due to the disordering of the electrons, it will be difficult to obtain the electric fields analytically. To find out the injection condition and injection threshold, we neglect the beam loading effects of the refluxing electrons after they cross with the outermost oscillating electron, i.e. they do not contribute to the electric field and disturb the motions of oscillating electrons. We can make this assumption because near the injection threshold, the injected charge is small and the beam loading effects are not significant. With this assumption, the electric force of the refluxing electrons can be obtained using the quasistatic theory[1] and their trajectories can be computed after sheet crossing as shown in Fig. 1(b). As a reference, the trajectories obtained from a 1D PIC simulations with the same parameters are shown in Fig. 1(c), and one can see the dynamics of the injected electrons are much alike despite the approximations we have made. Refluxing electrons can be injected into plasma waves if they are above the separatrix of injection when they cross with the outermost oscillating electron[1, 38]. The momentum of the outermost oscillating electron at sheet crossing moment is $p_{os} = -p_m \cos[\omega_\gamma(t_{sc} - \delta_m/v_d - t_0)]$, the separatrix of injection can be written as $p_{sp} = \left[v_d D - \sqrt{D^2 - (1 - v_d^2)} \right] / (1 - v_d^2)$, where $D = \sqrt{1 - v_d^2} - \sqrt{1 + p_m^2} + \sqrt{1 + p_{os}^2} + v_d(p_m - p_{os})$. The momentum of refluxing electron at sheet crossing time t_{re} is $p_{re} = p_m \cos[\omega_\gamma(t_{sc} - x_0/v_d - t_{re} - t_0)]$, and the injection condition can be thus written as

$$p_{re} - p_{sp} > 0. \quad (4)$$

The sheet crossing time t_{sc} and momentum difference $p_{re} - p_{sp}$ against different initial position x_0 are plotted in Fig. 2(a). As one can see, there are several separated injection areas with $p_{re} - p_{sp}$ above zero, and according to the corresponding t_{sc} (with the time reference of Fig. 1), we can tell that electrons from these

injection area are loaded into different acceleration buckets of the wakefields. Different from self-injection and downramp injection[1, 38], REI can not load electrons into the first acceleration bucket. The second acceleration bucket has the longest injection length and highest injected charge. Theoretical injection length of the second bucket as a function of normalized laser amplitude a_0 is shown in Fig. 2(b) together with numerical results from 1D and 3D PIC simulations with different laser waists (gaussian transverse profiles). The injection threshold, or the minimum a_0 required for injection, is about 1.05 according to the theory and 1D PIC simulations. The 1D PIC injection length is smaller than the theory for a_0 larger than the injection threshold. This is caused by the beam loading effects of injected bunch, which we neglected in our theoretical model. Due to the beam loading, the amplitudes of wakefields will be reduced and injected charge will be limited. The injection thresholds of 3D PIC simulations are larger than that of the 1D theory and simulation and with the decrease of the laser waist, the threshold increases. Because of the transverse ponderomotive force of the gaussian pulse, electrons are pushed away from the laser axis and the electric fields experienced by electrons are actually smaller than the on-axis value, which increases the threshold for injection. According to the 3D simulations, the power threshold for REI is $P/P_c \sim 1.4$ (varies for different densities, $P_c \simeq 17.5 n_c/n_0$ [GW] is the critical power for self-focusing), which is much smaller than that of self-injection measured at similar plasma densities ($P/P_c \sim 3$)[14]. For typical plasma densities used in LWFA ($10^{18} \sim 10^{19} \text{ cm}^{-3}$), the injection threshold increases with the decrease of the plasma density, but the variations are small as shown in Fig. 2(c). For more realistic vacuum-plasma transitions, we can model the density profile with $n_0(x) = H(x+l)H(-x)(x+l)/l + H(x)$, where l is the length of a linear density ramp. For small ramp lengths, the injection thresholds are similar to the ideal case we discussed above, as depicted in Fig. 2(d). When ramp length is longer than k_p^{-1} , the injection threshold almost linearly increases with the ramp length (Fig. 2(d)). For the ideal case, the refluxing electrons are injected into quasistatic plasma waves (wakes), the phase velocity of the wakes is approximately the group velocity of the laser. But for the long ramp cases, the refluxing electrons are injected into plasma waves with decreasing wavelengths. The equivalent phase velocity of the wakes can be much larger than light velocity and the injection thresholds are larger than the ideal case. When the transition is not from vacuum to plasma but from a low density plasma to a higher density one, the injection threshold also increases with the density ratio of the transition, as shown in Fig. 2(e). The injection threshold of the third bucket also changes due to the change of the ramp length or density ratio. Typically, the injection threshold of the third bucket is smaller than that of the second if the ramp length or density ratio is larger than zero.

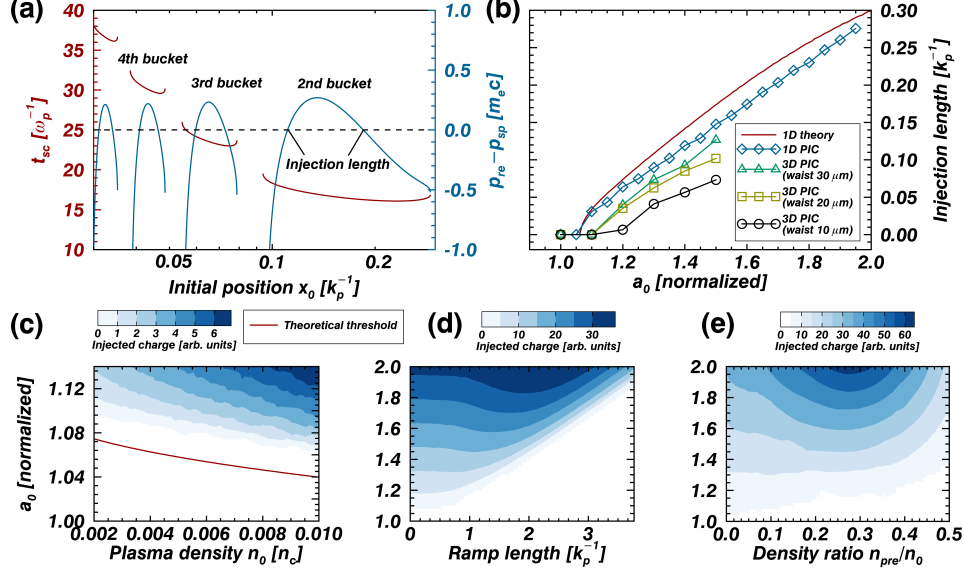


FIG. 2. (a) Reflexing time t_{sc} and momentum difference $p_{re} - p_{sp}$ as a function of electron initial position x_0 . The laser a_0 is 1.2. (b) Injection length of second bucket for different laser peak amplitude a_0 . (c) Injected charge in second bucket for different a_0 and plasma density n_0 . The red line is the theoretical threshold calculated by solving $\max(p_{re} - p_{sp}) = 0$. (d) Injected charge in second bucket for different a_0 and boundary ramp length. (e) Injected charge in second bucket for different a_0 and density ratio of a transition from plasma with density n_{pre} to plasma with density n_0 . Plasma density $n_0/n_c = 0.004$ is used for (a), (b), (d) and (e).

The beam qualities are determined by the electron distributions in six-dimensional phase space (x, y, z, p_x, p_y, p_z) [40]. The initial distributions of injected electrons in real space, or the collection volume must be well-confined to produce beams of high qualities[15]. For REI, the electron distribution after injection and the collection volume are shown in Figs. 3(a) and (b), respectively. The longitudinal bunch length is one order of magnitude larger than the injection length because of the differences in refluxing time for different initial positions. The collection volume will increase (in larger radius and longer injection length) with the increase of the laser amplitude or waist. The injected charge and current will also increase (Table I). To control the collection volume, it is favorable to operate the injection near the threshold. The injected bunch is negative chirped but the slice energy spread is very low, as shown in Fig. 3(c) and Table I. The front of the bunch are inside the focusing part of the wakefields and can preserve the beam qualities in acceleration[1]. Electrons in the rear are inside the defocusing part and they will eventually leave the acceleration region. The current profile is shown in Fig. 3(d), which is close to a flat-top profile. Before sheet crossing, the transverse momentums of refluxing electrons are small ($\sim 0.1 m_e c$)[39]. And when electrons are injected into the wakes, they start the well-known betatron oscillations due to the transverse focusing forces of the wakes[30]. Because the injection happens in a period of time ($\sim \omega_p^{-1}$)

w [μm]	10			20			30		
a_0	1.3	1.4	1.5	1.3	1.4	1.5	1.3	1.4	1.5
B_n [10^{16} A/m 2]	0.474	1.50	3.68	16.7	3.97	1.27	2.55	1.51	0.780
I [kA]	0.491	1.12	1.92	3.38	6.05	7.31	8.45	14.9	17.6
Q [pC]	1.19	3.67	7.36	11.0	24.5	40.3	27.2	55.9	90.7
τ [fs]	2.60	3.87	4.74	4.07	5.07	6.80	3.87	4.74	5.94
ε_{ny} [μm]	0.466	0.361	0.338	0.231	0.641	1.17	0.934	1.51	2.13
ε_{nz} [μm]	0.444	0.413	0.308	0.175	0.477	0.980	0.710	1.31	2.11
$\sigma_{\gamma s}$ [MeV]	0.200	0.118	0.214	0.275	0.660	1.14	0.631	1.15	1.64

TABLE I. Beam parameters of REI after propagating about 200 μm in plasma obtained from 3D PIC simulations. w is the laser waist, B_n is the peak brilliance, I is the peak current, Q is the injected charge (with $p_x/m_e c$ above 20) in the second bucket, τ is the FWHM bunch duration, ε_{ny} and ε_{nz} are normalized emittances in y and z directions, $\sigma_{\gamma s}$ is the averaged RMS slice energy spread. The slice length is chosen as 20 nm, and the slice energy spread is averaged over all slices within the FWHM of the current profile. The wavelength of driving laser is 800 nm and the plasma density is $0.004 n_c$.

much smaller than the period of betatron oscillations ($\sim \sqrt{\gamma} \omega_p^{-1}$)[30], the betatron phases of the injected electrons will be similar (Fig. 3(e)), which results in pretty small transverse emittances (0.1-1 μm) and high brilliances ($\sim 10^{16}$ A/m 2), as shown in Table I. The overall beam qualities of REI bunches are comparable to the beams driving free electron lasers[40].

REI is easier to be realized in lower density plasmas, because the required boundary ramp length can be

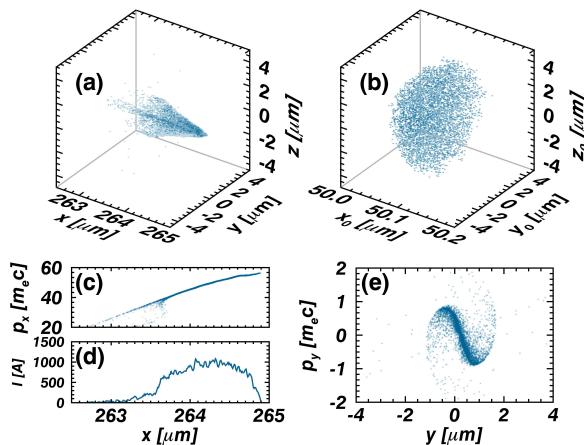


FIG. 3. 3D PIC simulation results of the REI electron bunch after propagating about $200 \mu\text{m}$ in plasma. The electrons are the same group of electrons in Table I with $a_0=1.4$, $w=10 \mu\text{m}$. (a) Positions of injected electrons. (b) Initial positions of injected electrons. The plasma boundary locates at $x = 50 \mu\text{m}$. (c) Longitudinal phasespace distribution of injected electrons. (d) Current profile of the injected bunch. (e) Transverse (along the laser polarization direction) phasespace distribution of the injected electrons. The wavelength of driving laser is 800 nm and the plasma density is $0.004n_c$.

larger. The beam qualities of REI can be well-preserved in the following acceleration with the scheme using different plasma densities for injection and acceleration[41]. Manipulating the energy chirp of the injected bunch[42, 43], we can also control the energy spread of the beam. REI can also be applied in a staged laser plasma

accelerator[44], considering the small threshold required for injection.

In summary, the dynamic process of a laser or particle beam propagating from vacuum into underdense plasma has been investigated theoretically. With a Lagrangian fluid model combined with the classic quasistatic wakefield theory, we found that background electrons can be injected into wakefields because sharp vacuum-plasma transitions can reduce the injection threshold. The injection condition, injection threshold as well as the injection length can be given theoretically by our model and are compared with results from computer simulations. Electron beams of high qualities can be produced near the injection thresholds and the proposed scheme is promising in reducing the injection threshold and improving the beam qualities of plasma based accelerators.

ACKNOWLEDGMENTS

The authors want to thank Antonio Ting for useful discussion. The PIC simulations were carried out in Shanghai Super Computation Center and Max Planck Computing and Data Facility. This work was supported by National Basic Research Program of China (Grant No. 2013CBA01502), National Natural Science Foundation of China (Grant Nos. 11575011, 11535001) and National Grand Instrument Project (2012YQ030142). The EPOCH program was funded by the UK EPSRC grants EP/G054950/1, EP/G056803/1, EP/G055165/1 and EP/M022463/1. J. Yu wants to thank the Project 2016M600007 funded by China Postdoctoral Science Foundation.

-
- [1] E. Esarey, C. B. Schroeder, and W. P. Leemans, *Rev. Mod. Phys.* **81**, 1229 (2009).
 - [2] T. Tajima and J. M. Dawson, *Phys. Rev. Lett.* **43**, 267 (1979).
 - [3] P. Chen, J. M. Dawson, R. W. Huff, and T. Katsouleas, *Phys. Rev. Lett.* **54**, 693 (1985).
 - [4] P. Muggli *et al.*, *Phys. Rev. Lett.* **93**, 014802 (2004).
 - [5] M. J. Hogan *et al.*, *Phys. Rev. Lett.* **95**, 054802 (2005).
 - [6] I. Blumenfeld *et al.*, *Nature* **445**, 741 (2007).
 - [7] M. Litos *et al.*, *Nature* **515**, 92 (2014).
 - [8] H. T. Kim, K. H. Pae, H. J. Cha, I. J. Kim, T. J. Yu, J. H. Sung, S. K. Lee, T. M. Jeong, and J. Lee, *Phys. Rev. Lett.* **111**, 165002 (2013).
 - [9] X. Wang, R. Zgadzaj, N. Fazel, Z. Li, S. A. Yi, X. Zhang, W. Henderson, Y. Y. Chang, R. Korzekwa, and H. E. Tsai, *Nature Comm.* **4**, 1988 (2013).
 - [10] W. Leemans, A. Gonsalves, H. S. Mao, K. Nakamura, C. Benedetti, C. Schroeder, C. Tóth, J. Daniels, D. Mittelberger, and S. Bulanov, *Phys. Rev. Lett.* **113**, 245002 (2014).
 - [11] W. Lu, M. Tzoufras, C. Joshi, F. S. Tsung, W. B. Mori, J. Vieira, R. A. Fonseca, and L. O. Silva, *Phys. Rev. ST Accel. Beams* **10**, 061301 (2007).
 - [12] I. Kostyukov, E. Nerush, A. Pukhov, and V. Seredov, *Phys. Rev. Lett.* **103**, 175003 (2009).
 - [13] S. Kalmykov, S. A. Yi, V. Khudik, and G. Shvets, *Phys. Rev. Lett.* **103**, 135004 (2009).
 - [14] D. H. Froula, C. E. Clayton, T. Döppner, K. A. Marsh, C. P. J. Barty, L. Divol, R. A. Fonseca, S. H. Glenzer, C. Joshi, and W. Lu, *Phys. Rev. Lett.* **103**, 215006 (2009).
 - [15] S. Corde, C. Thauray, A. Lifschitz, G. Lambert, K. T. Phuoc, X. Davoine, R. Lehe, D. Douillet, A. Rousse, and V. Malka, *Nature Comm.* **4**, 1501 (2013).
 - [16] C. G. R. Geddes, K. Nakamura, G. R. Plateau, C. Toth, E. Cormier-Michel, E. Esarey, C. B. Schroeder, J. R. Cary, and W. P. Leemans, *Phys. Rev. Lett.* **100**, 215004 (2008).
 - [17] K. Schmid, A. Buck, C. M. S. Sears, J. M. Mikhailova, R. Tautz, D. Herrmann, M. Geissler, F. Krausz, and L. Veisz, *Phys. Rev. ST Accel. Beams* **13**, 091301 (2010).
 - [18] A. Buck, J. Wenz, J. Xu, K. Khrennikov, K. Schmid, M. Heigoldt, J. M. Mikhailova, M. Geissler, B. Shen, and

- F. Krausz, Phys. Rev. Lett. **110**, 185006 (2013).
- [19] E. Esarey, R. F. Hubbard, W. P. Leemans, A. Ting, and P. Sprangle, Phys. Rev. Lett. **79**, 2682 (1997).
- [20] J. Faure, C. Rechatin, A. Norlin, A. Lifschitz, Y. Glinec, and V. Malka, Nature **444**, 737 (2006).
- [21] X. Davoine, E. Lefebvre, C. Rechatin, J. Faure, and V. Malka, Phys. Rev. Lett. **102**, 065001 (2009).
- [22] K. Kawase, L. M. Chen, A. Faenov, T. Pikuz, H. Kiriya, S. V. Bulanov, H. Kotaki, I. Daito, M. Kando, and Y. Hayashi, Phys. Rev. Lett. **103**, 194803 (2009).
- [23] R. Lehe, A. F. Lifschitz, X. Davoine, C. Thaury, and V. Malka, Phys. Rev. Lett. **111**, 085005 (2013).
- [24] A. Pak, K. A. Marsh, S. F. Martins, W. Lu, W. B. Mori, and C. Joshi, Phys. Rev. Lett. **104**, 025003 (2010).
- [25] C. E. Clayton *et al.*, Phys. Rev. Lett. **105**, 105003 (2010).
- [26] B. Hidding, G. Pretzler, J. B. Rosenzweig, T. Königstein, D. Schiller, and D. L. Bruhwiler, Phys. Rev. Lett. **108**, 035001 (2012).
- [27] N. Bourgeois, J. Cowley, and S. M. Hooker, Phys. Rev. Lett. **111**, 155004 (2013).
- [28] F. Li, J. F. Hua, X. L. Xu, C. J. Zhang, L. X. Yan, Y. C. Du, W. H. Huang, H. B. Chen, C. X. Tang, and W. Lu, Phys. Rev. Lett. **111**, 015003 (2013).
- [29] L. L. Yu, E. Esarey, C. B. Schroeder, J. L. Vay, C. Benedetti, C. G. R. Geddes, M. Chen, and W. P. Leemans, Phys. Rev. Lett. **112**, 125001 (2014).
- [30] X. L. Xu, J. F. Hua, F. Li, C. J. Zhang, L. X. Yan, Y. C. Du, W. H. Huang, H. B. Chen, C. X. Tang, and W. Lu, Phys. Rev. Lett. **112**, 035003 (2014).
- [31] X. L. Xu, *et al.*, Phys. Rev. ST Accel. Beams **17**, 061301 (2014).
- [32] M. Zeng, M. Chen, L. L. Yu, W. B. Mori, Z. M. Sheng, B. Hidding, D. A. Jaroszynski, and J. Zhang, Phys. Rev. Lett. **114**, 084801 (2015).
- [33] M. Mirzaie, S. Li, M. Zeng, N. A. M. Hafz, M. Chen, G. Y. Li, Q. J. Zhu, H. Liao, T. Sokollik, and F. Liu, Sci. Rep. **5**, 14659 (2015).
- [34] C.-T. Hsieh, C.-M. Huang, C.-L. Chang, Y.-C. Ho, Y.-S. Chen, J.-Y. Lin, J. Wang, and S.-Y. Chen, Phys. Rev. Lett. **96**, 095001 (2006).
- [35] M. H. Helle, D. F. Gordon, D. Kaganovich, Y. Chen, J. P. Palastro, and A. Ting, Phys. Rev. Lett. **117**, 165001 (2016).
- [36] J. M. Dawson, Phys. Rev. **113**, 383 (1959).
- [37] T. D. Arber, K. Bennett, C. S. Brady, A. Lawrence-douglas, M. G. Ramsay, N. J. Sircombe, P. Gillies, R. G. Evans, H. Schmitz, and A. R. Bell, Plasma Phys. Control. Fusion **57**, 113001 (2015).
- [38] J. Faure, CERN Yellow Reports **1**, 143 (2016).
- [39] See Supplemental Material at [URL will be inserted by publisher] for supplemental figures and detailed simulation parameters.
- [40] S. Di Mitri and M. Cornacchia, Phys. Rep. **539**, 1 (2014).
- [41] W. T. Wang *et al.*, Phys. Rev. Lett. **117**, 124801 (2016).
- [42] R. Brinkmann *et al.*, Phys. Rev. Lett. **118**, 214801 (2017).
- [43] R. Hu, H. Lu, Y. Shou, C. Lin, H. Zhuo, C.-e. Chen, and X. Yan, Phys. Rev. Accel. Beams **19**, 091301 (2016).
- [44] S. Steinke *et al.*, Nature **530**, 190 (2016).